RSC Advances

PAPER

View Article Online
View Journal | View Issue

Cite this: *RSC Adv.*, 2018, **8**, 5523

Effect of Ti-doping on the electrochemical performance of sodium vanadium(III) phosphate

Bao Zhang,[a] Tao Zeng,[a] Yi Liu[b] and Jia-feng Zhang *[a]

Received 24th November 2017
Accepted 22nd December 2017

DOI: 10.1039/c7ra12743j

rsc.li/rsc-advances

$Na_3V_{2-x}Ti_x(PO_4)_3$ ($x = 0.00$, 0.05, 0.10, and 0.15) was successfully synthesized by a conventional solid-state route. The XRD results show that Ti is incorporated in the lattice of $Na_3V_2(PO_4)_3$ and the tetragonal structure has not been changed after doping. Among all the composites, the $Na_3V_{1.9}Ti_{0.1}(PO_4)_3$ composite delivers the highest discharge capacity of 114.87 mA h g^{-1} at 0.1C and possesses a capacity retention of 96.23% after 20 cycles at 0.1C, demonstrating the better rate performance and cycle stability in the potential range of 2.0–3.8 V. Electrochemical impedance spectroscopy (EIS) results reveal that the $Na_3V_{1.9}Ti_{0.1}(PO_4)_3$ composite has a lower charge transfer resistance and a higher Na-ion diffusion coefficient compared to other composites. The results indicate that Ti-doping in $Na_3V_2(PO_4)_3$ can effectively enhance the electrochemical performance of this tetragonal compound, especially at a high charge/discharge rate.

1 Introduction

Since the combustion of fossil fuels results in air pollution and increases the greenhouse effect, much attention has been focused on the exploitation of new energy sources. Development of new alternative energy storage systems with low cost, high safety and environmentally friendly electrode materials are critical to meet our rising energy demands and, in particular, to facilitate the adoption of renewable energy generation. Large-scale electric energy storage is a key enabler for the use of renewable energy.[1] Lithium ion batteries with high energy and power densities have been considered as the best power sources for portable equipment today.[2–4] $LiFePO_4$, $FePO_4$, $LiMnPO_4$, $Li(Fe,Mn)PO_4$, $LiCoPO_4$, $LiNiPO_4$, $Li_3V_2(PO_4)_3$, and $LiCo_{1/2}Ni_{1/2}PO_4$, $LiCoO_2$, $LiNi_{1/3}Co_{1/3}Mn_{1/3}O_2$ have been researched as cathode materials for Li-ion batteries.[5–16] However, there is serious concern about the availability of lithium owing to the amount of lithium reserves in the earth, especially for large-scale applications.[17,18] On this occasion, the eco-friendly sodium-ion batteries have become the focus in the field of energy and environment due to the abundance of sodium.[17,19–21]

In recent years, many electrode materials such as Na_xCoO_2,[22] $Na_{0.44}MnO_2$,[23] NaV_6O_{15},[24] $Na_{1-x}Ni_{0.5}Mn_{0.5}O_2$,[25] $NaNi_{1/3}Mn_{1/3}Co_{1/3}O_2$,[26] $NaFePO_4$,[27] $NaFeSO_4F$,[28] $NaV_{1-x}Cr_xPO_4F$,[29] Na_2FePO_4F,[30] $Na_3V_2(PO_4)_2F_3$,[31] $Na_2Ti_3O_7$,[32,33] and $Na_2C_8H_4O_4$ (ref. 34) have been extensively investigated for sodium ion batteries. Recently, NASICON (for Na^+ superionic conductor)-type electrode materials that can generate large interstitial spaces, through which sodium ions can diffuse, have aroused much interest of many researchers.[35,36]

$Na_3V_2(PO_4)_3$ (NVP), which is a polyanionic material, has been greatly exploited[37] for its several advantages: (1) good ionic mobility, (2) a high theoretical specific capacity (117.6 mA h g^{-1}), (3) two very flat and stable redox electric potentials (3.4 and 1.6 V *vs.* Na^+/Na) based on the V^{4+}/V^{3+} and V^{3+}/V^{2+} redox couples, respectively. However, the stability of the structure of NVP also needs to be improved. It has been reported that transition metal doping is a useful way to improve the electrochemical performance of $Li_3V_2(PO_4)_3$.[38] Several cations, such as Fe^{3+},[39] Cr^{3+},[40] Mg^{2+},[41] Co^{2+},[42] and Ti^{4+},[43] can be doped at the V site in the LVP, resulting in improved utilization of materials, high rate capabilities, electric conductivity, and cyclic stability. In the present work, we investigate aliovalent substitution of V^{III} with Ti^{IV} in NVP. So far, no studies have been done to dope titanium in NVP. We examine the effect of low levels of Ti doping on the electrochemical performance of NVP. The addition of titanium did not influence the structure of NVP, but the particle size was reduced and the electrical conductivity was improved, resulting in high capacity and rate capability.

2 Experiment

2.1 Synthesis

The $Na_3V_{2-x}Ti_x(PO_4)_3$ ($x = 0.00$, 0.05, 0.10, 0.15) composites were synthesized by a conventional solid-state route. $NaH_2PO_4 \cdot 2H_2O$ and V_2O_5 were used as the starting materials and ethanedioic acid was used as the reductant. In a typical synthesis process, V_2O_5, $NaH_2PO_4 \cdot 2H_2O$, nano-size TiO_2, and $H_2C_2O_4$ (in the appropriate amount) were mixed and ball-milled with alcohol media in a container of a planetary ball-mill at

[a]School of Metallurgy and Environment, Central South University, Changsha, 410083, PR China. E-mail: yjyzjf@csu.edu.cn
[b]Tianjin Lishen Battery Joint-Stock Co., Ltd, Tianjin, 300384, PR China

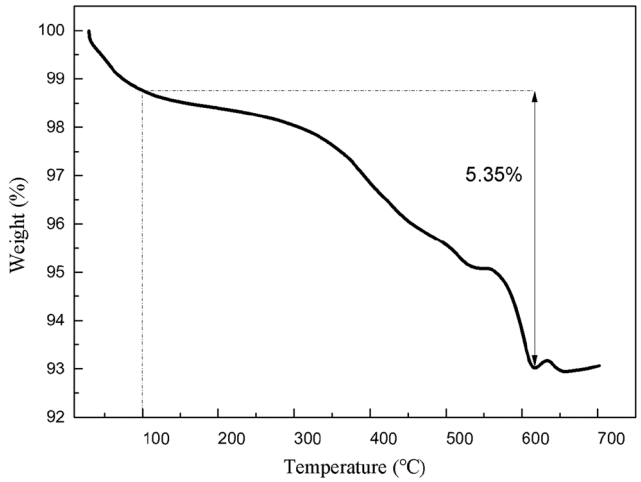

Fig. 1 The TGA curve of $Na_3V_{1.9}Ti_{0.1}(PO_4)_3$.

300 rpm for 5 h. After ball-milling, the obtained mixture was dried at 75 °C, then calcinated at 400 °C for 4 h and heated up to 750 °C and held there for 10 h in an atmosphere-controlled furnace under argon. The heating rate was 5 °C min^{-1}. The $Na_3V_{2-x}Ti_x(PO_4)_3$ (x = 0.00, 0.05, 0.10, 0.15) composites was obtained.

2.2 Material characterization

Thermogravimetric (TG/DSC) analysis of the mixture was measured on a SDT Q600 TG-DTA apparatus at temperature between 25 and 900 °C at a heating rate of 5 °C min^{-1} under argon flow. The powder X-ray diffraction (XRD, Rint-2000, Rigaku, Japan) measurement using Cu Kα radiation was employed to identify the crystalline phases of the synthesized composites. XRD Rietveld refinement was analyzed by software (MAUD). The morphologies and chemical compositions of the composites were observed by scanning electron microscopy (SEM, JEOL, JSM-5600LV, Japan) and a energy dispersive X-ray (EDX) detector.

2.3 Electrochemical performance tests

The cathodes used for the electrochemical tests consisted of 80 wt% active material, 10 wt% acetylene black, and 10 wt% polyvinylidene fluoride (PVDF), which was used as the binder. *N*-Methyl-2-pyrrolidone (NMP) was used as a solvent and an aluminum foil as a current collector (~2.0 mg cm^{-2}). It was dried in a vacuum oven at 120 °C for 4 h. Electrodes of the desired size were then punched out from the dried slurry. Electrochemical cells were assembled in a glove box filled with high-purity argon; pure sodium foil was used as the counter electrode. The electrolyte solution was 1 M $NaClO_4$ (EC:DEC) (1% VC) soaked in glass fiber separators (GF/D-Whatman). The test cells were galvanostatically cycled between 2.0 and 3.5 V. Na^+/Na at various C-rates based on the theoretical capacity of 118 mA h g^{-1}. The cyclic voltammetry (CV) profiles were recorded with a LK2005A electrochemical workstation (Lanlike Co., China). Electrochemistry impedance spectroscopy (EIS) was measured with an electrochemical workstation (CHI 660D) by applying an AC voltage of 5 mV in the frequency range from 100 kHz to 0.04 Hz.

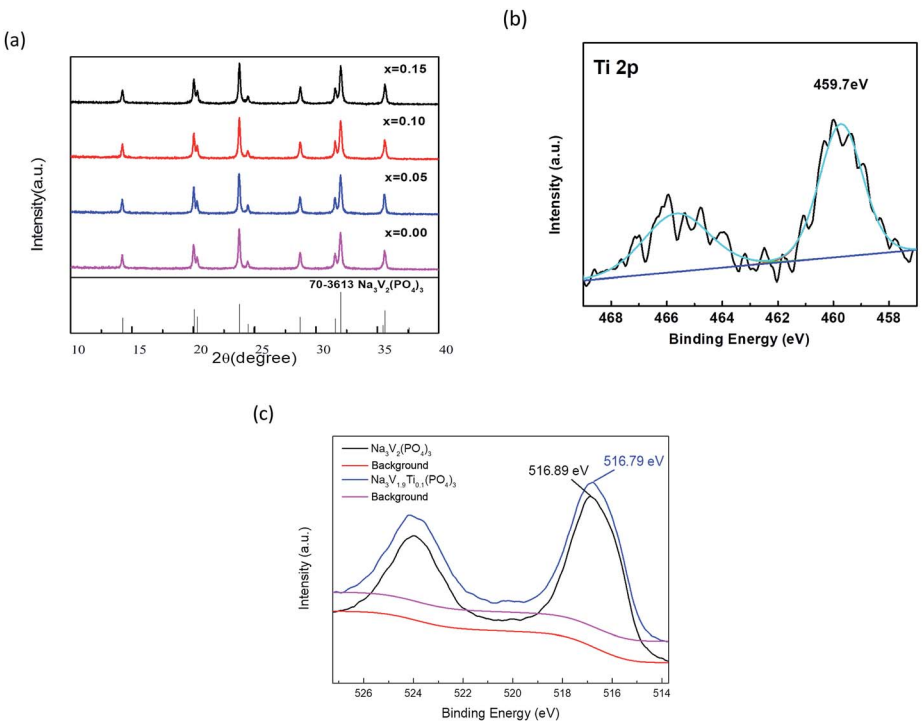

Fig. 2 (a) XRD patterns of $Na_3V_{2-x}Ti_x(PO_4)_3$ (x = 0.00, 0.05, 0.10, 0.15) with various doping amount, (b) the XPS spectra of Ti 2p ($Na_3V_{1.9}Ti_{0.1}(PO_4)_3$), (c) the XPS spectra of V 2p ($Na_3V_2(PO_4)_3$ and $Na_3V_{1.9}Ti_{0.1}(PO_4)_3$).

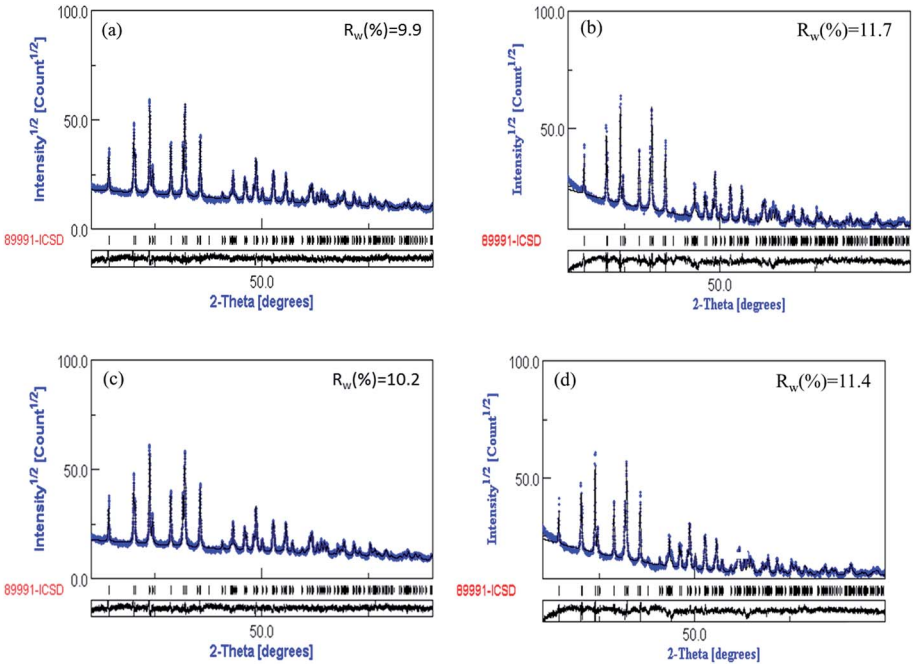

Fig. 3 Refinement XRD profiles for $Na_3V_{2-x}Ti_x(PO_4)_3$. (a) $x = 0.00$, (b) $x = 0.05$, (c) $x = 0.10$, (d) $x = 0.15$.

Table 1 Lattice parameters of the pristine $Na_3V_2(PO_4)_3$ and $Na_3V_{1.9}Ti_{0.1}(PO_4)_3$ samples

	a (Å)	c (Å)	Vol. (Å^3)	R_w (%)
$Na_3V_2(PO_4)_3$	8.72436	21.80602	1659.8	9.9
$Na_3V_{1.95}Ti_{0.05}(PO_4)_3$	8.72275	21.80401	1659.0	11.7
$Na_3V_{1.9}Ti_{0.1}(PO_4)_3$	8.71929	21.80088	1657.4	10.2
$Na_3V_{1.85}Ti_{0.15}(PO_4)_3$	8.72137	21.80135	1658.3	11.4

3 Results and discussion

Fig. 1 shows the TGA curve of $Na_3V_{1.9}Ti_{0.1}(PO_4)_3$. The TGA test was taken in the oxygen. It was observed that the carbon content in the $Na_3V_{1.9}Ti_{0.1}(PO_4)_3$ was 5.35%.

XRD patterns of $Na_3V_{2-x}Ti_x(PO_4)_3$ ($x = 0.00$, 0.05, 0.10, 0.15) with various amounts of Ti doping are shown in Fig. 2a. All the peaks are indexed to a single phase of tetragonal crystal type

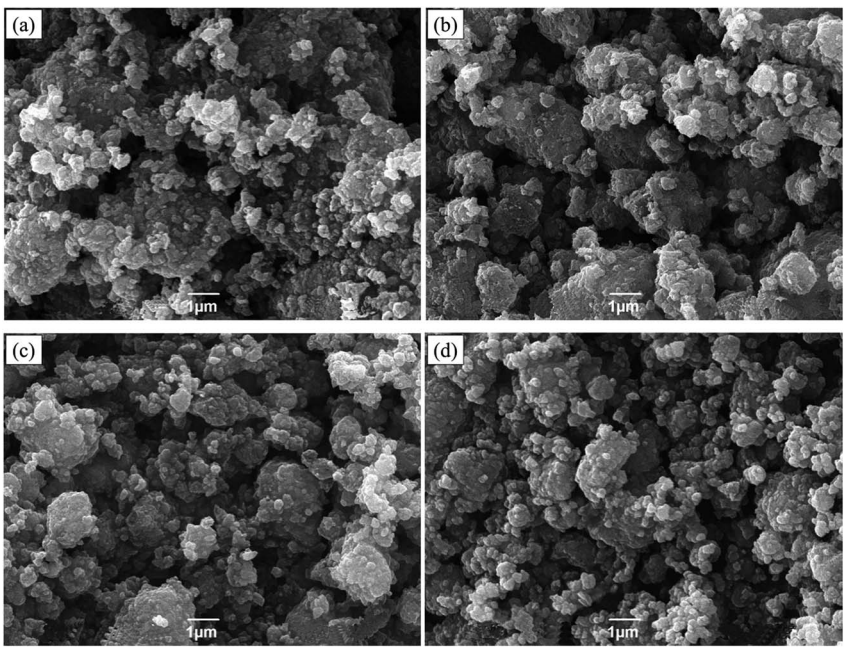

Fig. 4 SEM images of $Na_3V_{2-x}Ti_x(PO_4)_3$. (a) $x = 0.00$, (b) $x = 0.05$, (c) $x = 0.10$, (d) $x = 0.15$.

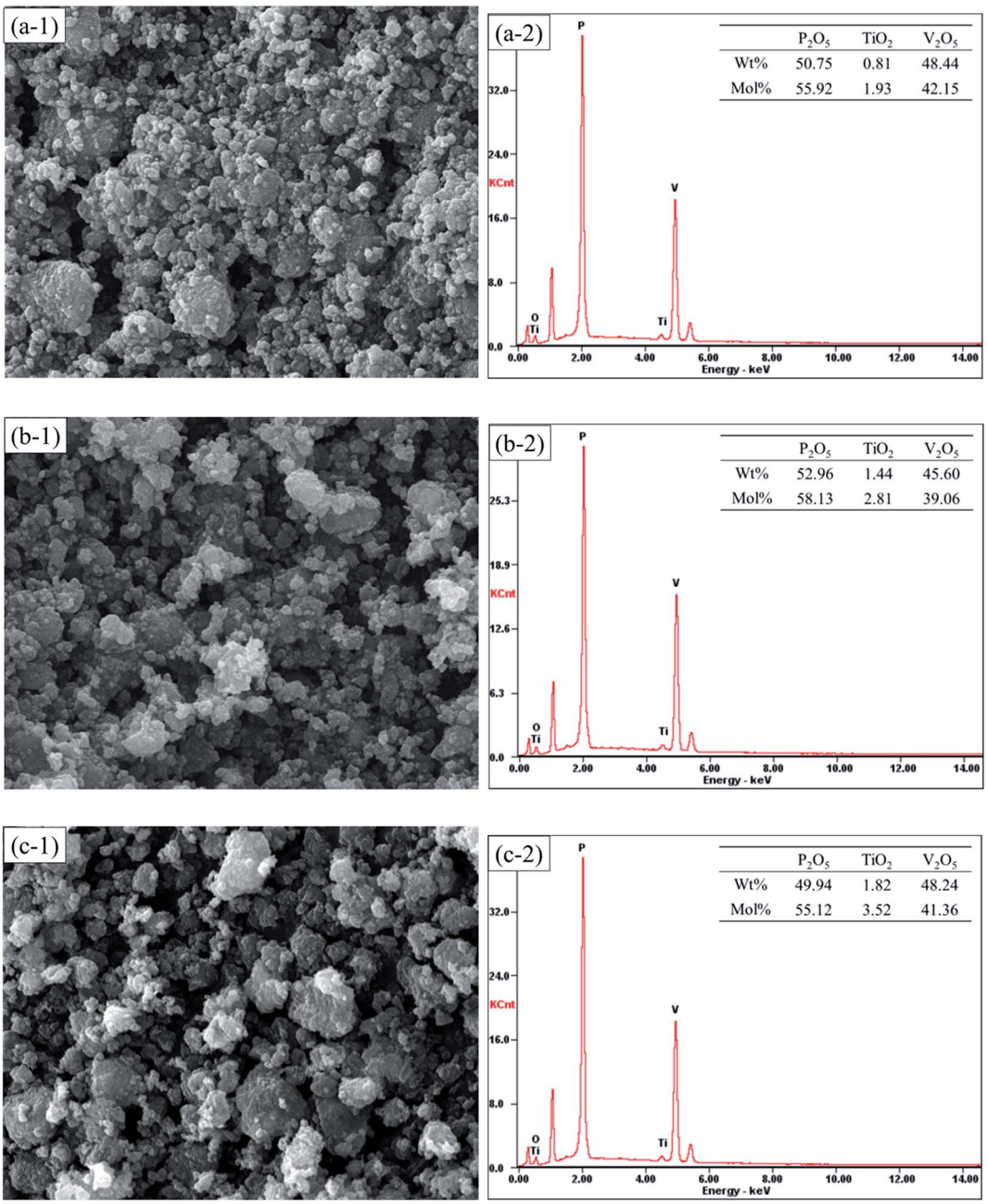

Fig. 5 EDX images of $Na_3V_{2-x}Ti_x(PO_4)_3$. (a) $x = 0.05$, (b) $x = 0.10$, (c) $x = 0.15$.

$Na_3V_2(PO_4)_3$, which is consistent with the references. It is clear that no impurity peaks such as Ti-doped composites are detected, indicating that the as-prepared composites are pure phase and the structure is unchanged after Ti doping. These sharp peaks in the patterns suggest good crystallinity of the powders.

The XPS spectra of Ti 2p ($Na_3V_{1.9}Ti_{0.1}(PO_4)_3$) was shown in Fig. 2b. The binding energy of Ti in the picture to be 459.7 eV, matched well with some previous work,[44] which indicate the valence of Ti in $Na_3V_{1.9}Ti_{0.1}(PO_4)_3$ is +4. The XPS spectra of V 2p ($Na_3V_2(PO_4)_3$ and $Na_3V_{1.9}Ti_{0.1}(PO_4)_3$) was shown in Fig. 2c. It is obviously that the binding energy of V in Ti-doping sample ($Na_3V_{1.9}Ti_{0.1}(PO_4)_3$) is 516.79 eV and the binding energy of V in $Na_3V_2(PO_4)_3$ is 516.89 eV, which means that the doping of titanium reduce the valence of V. The result means that Ti is doped in the V site.[45]

Fig. 3 show the refined XRD data for $Na_3V_{2-x}Ti_x(PO_4)_3$ (x = 0.00, 0.05, 0.10, 0.15). The calculated pattern matched well with the PDF standard card. The refined lattice parameters and atomic coordination are listed in Table 1. The R_w of Na_3V_{2-x}-$Ti_x(PO_4)_3$ (x = 0.00, 0.05, 0.10, 0.15) were 9.9%, 11.7%, 10.2% and 11.4%, respectively. The decrease of cell volume can be attributed to the insertion of Ti, which is consistent with the previous result.[44] As can be seen in Table 1 that the $Na_3V_{1.9}$-$Ti_{0.1}(PO_4)_3$ had the smallest volumes. This indicates that the $Na_3V_{1.9}Ti_{0.1}(PO_4)_3$ composites had smallest particle size.

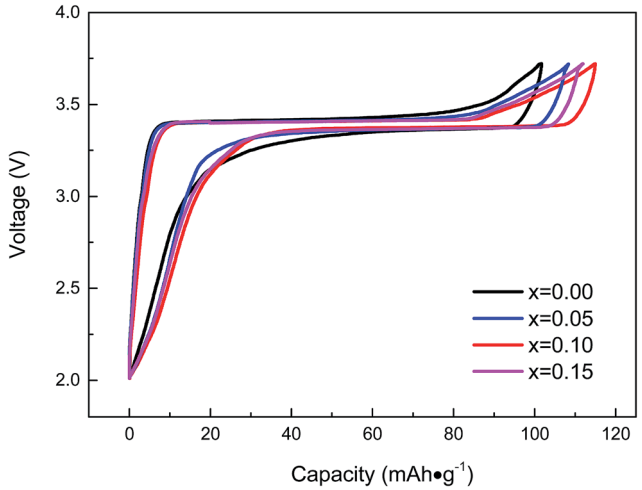

Fig. 6 Initial charge–discharge voltage profiles of $Na_3V_{2-x}Ti_x(PO_4)_3$ (x = 0.00, 0.05, 0.10, 0.15) at 0.1C.

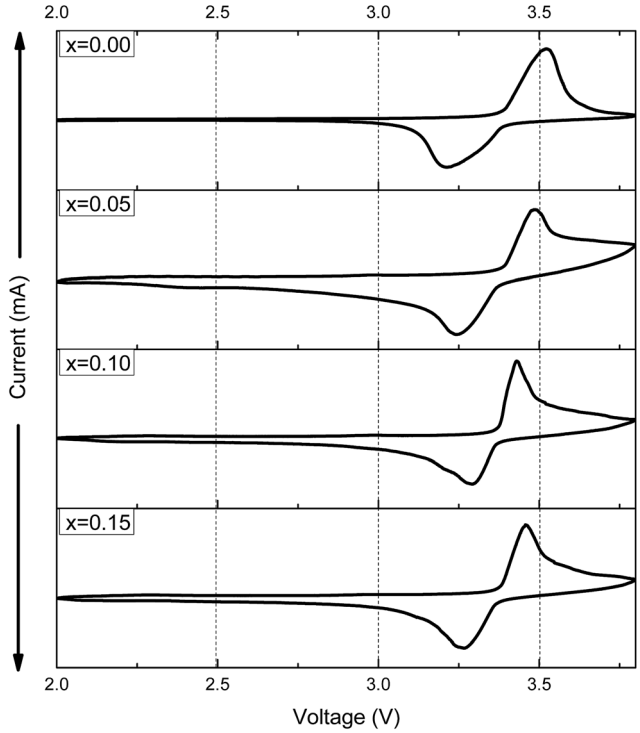

Fig. 7 CV curves of $Na_3V_{2-x}Ti_x(PO_4)_3$ (x = 0.00, 0.05, 0.10, 0.15) at 0.1C.

Fig. 4 shows the SEM images of $Na_3V_{2-x}Ti_x(PO_4)_3$ (x = 0.00, 0.05, 0.10, 0.15). It's observed that the primary particles are in nano-scale and agglomerated to form secondary particles, showing similar irregular granular shapes. The results indicate a more homogeneous distribution of Ti-doping composites than the pristine one.

Fig. 5 shows the SEM images of $Na_3V_{2-x}Ti_x(PO_4)_3$ (x = 0.00, 0.05, 0.10, 0.15). EDX was used to investigate the existed component elements in the composites. It can be seen in Fig. 5 that the element Ti is existed in $Na_3V_{2-x}Ti_x(PO_4)_3$ (x = 0.00, 0.05, 0.10, 0.15), and the contents of Ti gradually increases with the rise of Ti concentrations, indicating that the $Na_3V_{2-x}Ti_x(PO_4)_3$ (x = 0.00, 0.05, 0.10, 0.15) composites was successfully synthesized.

Fig. 6 shows the initial charge–discharge voltage profiles of $Na_3V_{2-x}Ti_x(PO_4)_3$ (x = 0.00, 0.05, 0.10, 0.15) at a current rate of 0.1C in the potential range of 2.0–3.8 V. The curves indicate that two Na ions were extracted from/inserted into $Na_3V_2(PO_4)_3$ per formula unit during the charging/discharging processes, which lasted for 10 h.[46] It can be seen from Fig. 6 that the charge curves for all cathodes exhibited a plateau at approximately 3.4 V and so did the corresponding discharge curves; these were attributed to the two-phase transitions occurring during the electrochemical reaction, which was agreed well with the CV curves as showed in Fig. 7. The initial discharge capacity of $Na_3V_{2-x}Ti_x(PO_4)_3$ composites (x = 0.00, x = 0.05, x = 0.10, x = 0.15) are 102.58 mA h g^{-1}, 107.63 mA h g^{-1}, 114.87 mA h g^{-1} and 111.95 mA h g^{-1}, respectively. The coulombic efficiency of the initial cycle is about 94.9%, 96.7%, 98.9% and 97.8%, respectively. As can be seen from Fig. 6 that the capacities of Ti-doped $Na_3V_{2-x}Ti_x(PO_4)_3$ (x = 0.00, 0.05, 0.10, 0.15) are higher than pristine $Na_3V_2(PO_4)_3$. In addition, the voltage difference of Ti-doped $Na_3V_{2-x}Ti_x(PO_4)_3$ is smaller than that of pristine $Na_3V_2(PO_4)_3$, resulting from the lower electrode polarization. It is clearly seen from Table 3 that $Na_3V_{1.9}Ti_{0.1}(PO_4)_3$ exhibits the lowest polarization potential of 0.03 V with the best electrochemical performance and the highest initial discharge capacity, indicating that Ti-doping does not block the tunnels of Na ions and probably increases the charge and discharge capacities and charge–discharge efficiency.

CV measurement was carried out at a scan rate of 0.1 mV s^{-1} to provide more information about the electrochemical properties, the second voltammograms (CV) of $Na_3V_{2-x}Ti_x(PO_4)_3$ (x = 0.00, 0.05, 0.10, 0.15) samples in the voltage range of 2.0–3.8 V are presented in Fig. 7. It can be observed that the CV curves are very similar. There are one oxidation peak and one reduction peak, corresponding to the relative Na^+ ion extraction and reinsertion. However, the Na^+ ion extraction and insertion processes for Ti doped samples are more stable, which is ascribed to relatively sharper peaks. Moreover, the $Na_3V_{1.9}Ti_{0.1}(PO_4)_3$ sample present the smallest potential differences between anodic and cathodic peaks, which is consistent with the result in charge–discharge voltage profiles, indicating the good reversibility of the Na^+ ion extraction/re-insertion and lower ohmic resistance in the electrode.

As shown in Fig. 8, five current densities, *i.e.* 0.1C, 0.5C, 1C, 2C and 5C, are employed to evaluate the rate capability of $Na_3V_{2-x}Ti_x(PO_4)_3$ (x = 0.00, 0.05, 0.10, 0.15) (charging current density is 0.1C). It can be observed that the profiles reveal a large plateau at 3.4 V for discharge and the rate performance of the composites is highly affected by the Ti-doped content. Increasing Ti-doping amount first led to the enhancement of rate capability. It can be seen in Fig. 8 that Ti-doping samples show better rate performance than pristine $Na_3V_2(PO_4)_3$. Moreover, $Na_3V_{1.9}Ti_{0.1}(PO_4)_3$ shows the best rate performance, delivering a capacity of 114.87 mA h g^{-1}, 113.75 mA h g^{-1},

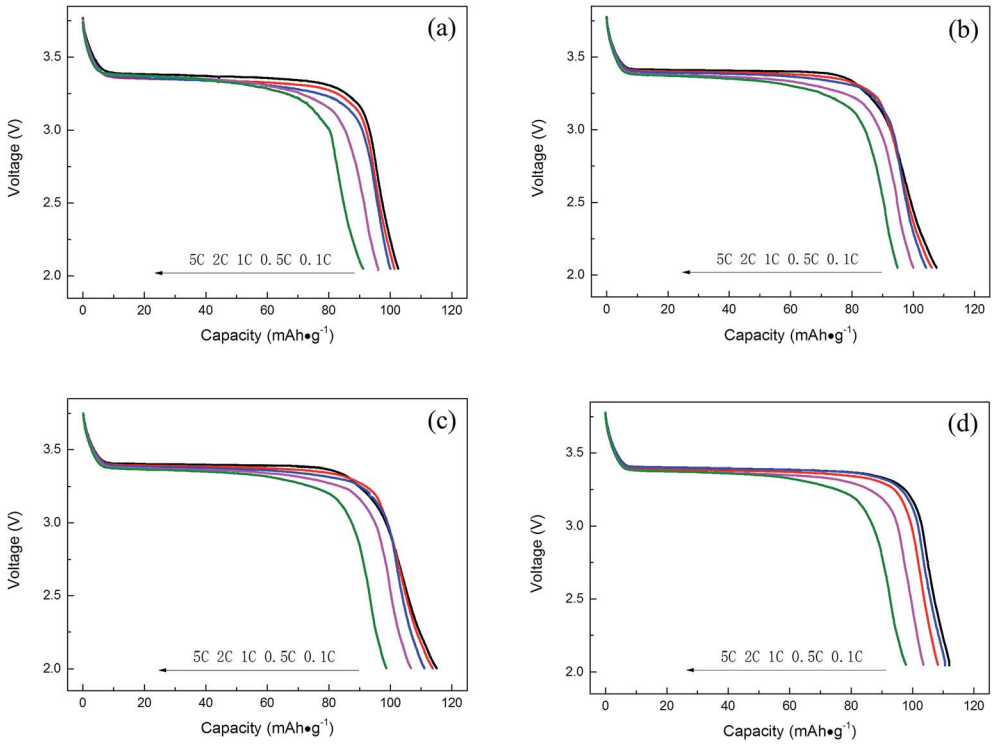

Fig. 8 The discharge curves of $Na_3V_{2-x}Ti_x(PO_4)_3$ (x = 0.00, 0.05, 0.10, 0.15) at various rates. (a) x = 0.00, (b) x = 0.05, (c) x = 0.10, (d) x = 0.15.

111.07 mA h g^{-1}, 106.67 mA h g^{-1}, and 98.63 mA h g^{-1}. Moreover, the discharge voltage plateau of $Na_3V_{1.9}Ti_{0.1}(PO_4)_3$ is still higher than 3.3 V at 5C rate, indicating that $Na_3V_{1.9}Ti_{0.1}(PO_4)_3$ has a lower polarization. The results prove that Ti-doping can enhance the electrochemical performance.

All the $Na_3V_{2-x}Ti_x(PO_4)_3$ (x = 0.00, 0.05, 0.10, 0.15) samples were cycled at five current densities (0.1, 0.5, 1, 2, and 5C) between 2.0 and 3.8 V, and the results are shown in Fig. 9a. Each current density was tested for 5 cycles. It can be observed that the Ti-doping samples show a better rate performance than pristine $Na_3V_2(PO_4)_3$. Even so, a further increase of the titanium content was not as advantageous as for the former samples. Moreover, the rate performance of $Na_3V_{1.9}Ti_{0.1}(PO_4)_3$ demonstrates the best among all samples, and it keeps a 97.02% at all rates, higher than that of the others. The sample with suitable Ti-doping content (x = 0.10) shows the best rate performance compared with other samples. The results proved that Ti-doping can improve the rate performance of $Na_3V_2(PO_4)_3$.

Fig. 9b shows the cycling performance of $Na_3V_{2-x}Ti_x(PO_4)_3$ (x = 0.00, 0.05, 0.10, 0.15) electrodes at 0.5C. As can be seen from Fig. 9b that the Ti-doping samples, expect $Na_3V_{2-x}Ti_x(PO_4)_3$ (x = 0.05), show a better cycling performance than pristine $Na_3V_2(PO_4)_3$. The discharge capacity of $Na_3V_{2-x}Ti_x(PO_4)_3$ composites (x = 0.00, x = 0.05, x = 0.10, x = 0.15) are 101.83 mA h g^{-1}, 106.02 mA h g^{-1}, 113.75 mA h g^{-1} and 110.59 mA h g^{-1}, respectively, and 94.59%, 93.44%, 96.70% and 95.25% remained after 100 cycles in the range of 2.0–3.8 V at 0.5C. The results indicate that suitable Ti-doping content (x = 0.10, x = 0.15) can enhance the cycling performance of $Na_3V_2(PO_4)_3$.

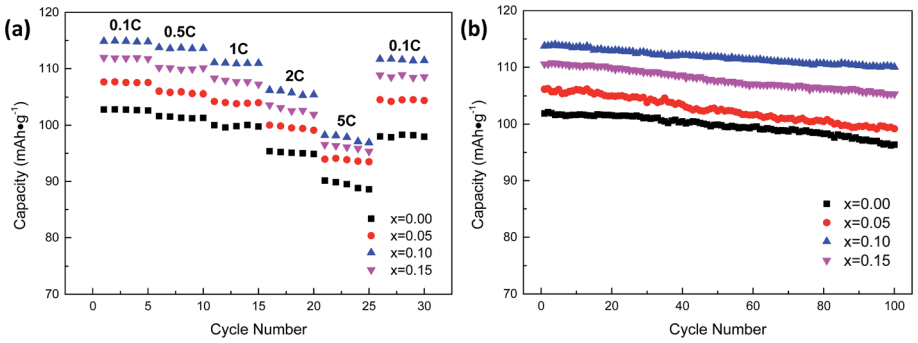

Fig. 9 (a) Discharge capacities of $Na_3V_{2-x}Ti_x(PO_4)_3$ (x = 0.00, 0.05, 0.10, 0.15) samples at current densities of 0.1C, 0.5C, 1C, 2C and 5C in the voltage range of 2.0–3.8 V, (b) cycling performance of $Na_3V_{2-x}Ti_x(PO_4)_3$ (x = 0.00, 0.05, 0.10, 0.15) electrodes at 0.5C.

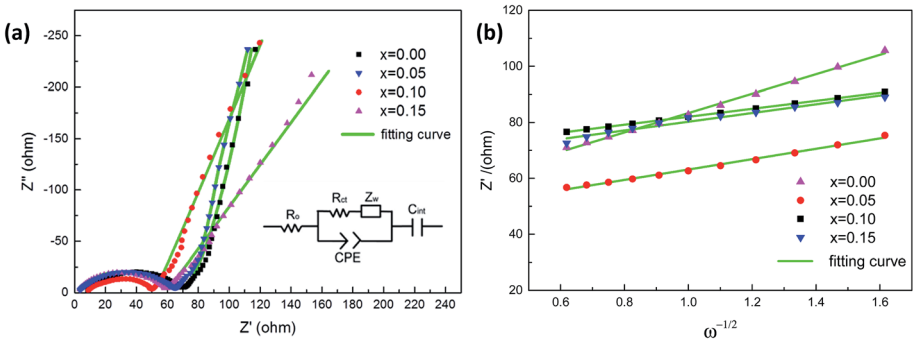

Fig. 10 (a) Nyquist plots of $Na_3V_{2-x}Ti_x(PO_4)_3$ ($x = 0.00, 0.05, 0.10, 0.15$). Inset shows an equivalent circuit adopted to simulate the impedance spectra, (b) relationship between Z_0 and $\omega^{-1/2}$ in the low frequency region of $Na_3V_{2-x}Ti_x(PO_4)_3$ ($x = 0.00, 0.05, 0.10, 0.15$).

Table 2 EIS simulation parameters of $Na_3V_{2-x}Ti_x(PO_4)_3$ ($x = 0.00, 0.05, 0.10, 0.15$)

Samples	R_o (Ω cm^{-2})	R_{ct} (Ω cm^{-2})	D_{Na} (10^{-16})
$x = 0.00$	7.36	61.01	5.98
$x = 0.05$	2.44	59.35	11.49
$x = 0.10$	7.41	44.75	14.53
$x = 0.15$	2.20	53.87	13.27

Fig. 10a presents the AC impedance spectra of $Na_3V_{2-x}Ti_x(PO_4)_3$ ($x = 0.00, 0.05, 0.10, 0.15$). The spectras show an intercept at a high frequency, followed by a depressed semicircle in the high-middle frequency region, and a straight line in the low frequency region. An equivalent circuit was conducted to refine the spectra. In the circuit, R_o represents the ohmic resistance of the electrolyte and electrode, as the intercept impedance on the Z-axis. CPE represents the double layer capacitance. R_{ct} is the charge transfer resistance, Z_w represents the diffusion-controlled Warburg impedance, and C_{int} indicates the capacitance caused by the cumulation or loss of Na^+ in the crystal of electrode material. The parameters obtained from the equivalent circuit fitting are shown in Table 2. It is found that the R_{ct} of $Na_3V_{2-x}Ti_x(PO_4)_3$ composites with $x = 0.00$, $x = 0.05$, $x = 0.10$, $x = 0.15$ are 61.01 Ω, 59.35 Ω, 44.75 Ω and 53.87 Ω, respectively, which indicates that Ti-doping can increase the charge transfer speed of the electrochemical reaction. Moreover, the minimum R_{ct} of $Na_3V_{1.9}Ti_{0.1}(PO_4)_3$ results in its best electrochemical performance among all the samples.

The diffusion coefficient of lithium ions (D_{Na}) are calculated by equations. The results are also summarized in Table 2.

$$D_{Na} = \frac{R^2T^2}{2A^2F^4C_{Na}{}^2\delta^2}$$

Table 3 The initial charge–discharge overpotential of $Na_3V_{2-x}Ti_x(PO_4)_3$ ($x = 0.00, 0.05, 0.10, 0.15$)

Samples	$x = 0.00$	$x = 0.05$	$x = 0.10$	$x = 0.15$
Overpotential (V)	0.11	0.06	0.03	0.05

where R, the gas constant, T, the absolute temperature, A, the surface area of the cathode, the number of electrons involved in the redox process, F, Faraday's constant, C_{Na}, the concentration of sodium ion, so δ is the slope for the plot of Z' *versus* the reciprocal square root of the lower angular frequencies ($\omega^{-1/2}$). To obtain the Warburg coefficient (δ), the linear fitting of Z' *versus* $\omega^{-1/2}$ is shown in Fig. 10b. All the parameters are listed in Table 2. It is seen that $Na_3V_{1.9}Ti_{0.1}(PO_4)_3$ exhibit the highest value of D_{Na} among all the samples, which indicates that the electrochemical property of $Na_3V_2(PO_4)_3$ composites can be improved by an appropriate amount of Ti ion doping.

4 Conclusion

The $Na_3V_{2-x}Ti_x(PO_4)_3$ ($x = 0.00, 0.05, 0.10, 0.15$) was successfully synthesized by a conventional solid state route. Based on the XRD refinement results, Ti has incorporated into the lattice of $Na_3V_2(PO_4)_3$. The amount of Ti doping has an important impact on electrochemical performance. In the electrochemical test, $Na_3V_{1.9}Ti_{0.1}(PO_4)_3$ exhibits the best specific capacity of 114.87 mA h g^{-1} at 0.1C in the potential range of 2.0–3.8 V and possessing the capacity retention of 96.70% after 100 cycles at 0.5C. The Ti-added $Na_3V_2(PO_4)_3$ composites also show higher rate capability and cycle performance compared with the pristine $Na_3V_2(PO_4)_3$. The results of CV and EIS revealed that the doping titanium at an appropriate amount could increase the diffusion coefficient of sodium ions and result in the improvement of the reversibility of the materials. The results indicate that the Ti doping is an effective approach to achieve excellent electrochemical performance for the sodium ion pyrophosphate.

Conflicts of interest

There are no conflicts to declare.

Acknowledgements

We gratefully acknowledge the financial support for this work of the National Natural Science Foundation of China (General Program) under grant number 51272290 and 51402365.

References

1 T. Ramireddy, M. M. Rahman, N. Sharma, *et al.*, Carbon coated $Na_7Fe_7(PO_4)_6F_3$: A novel intercalation cathode for sodium-ion batteries, *J. Power Sources*, 2014, **271**, 497–503.

2 C. Sun, S. Rajasekhara, J. B. Goodenough, *et al.*, Monodisperse Porous $LiFePO_4$ Microspheres for a High Power Li-Ion Battery Cathode, *J. Am. Chem. Soc.*, 2011, **133**(7), 2132–2135.

3 Y. Janssen, D. S. Middlemiss, S. Bo, *et al.*, Structural Modulation in the High Capacity Battery Cathode Material $LiFeBO_3$, *J. Am. Chem. Soc.*, 2012, **134**(30), 12516–12527.

4 M. Konarova and I. Taniguchi, Synthesis of carbon-coated $LiFePO_4$ nanoparticles with high rate performance in lithium secondary batteries, *J. Power Sources*, 2010, **195**(11), 3661–3667.

5 E. Kobayashi, L. S. Plashnitsa, T. Doi, *et al.*, Electrochemical properties of Li symmetric solid-state cell with NASICON-type solid electrolyte and electrodes, *Electrochem. Commun.*, 2010, **12**(7), 894–896.

6 A. Pan, D. Choi, J. Zhang, *et al.*, High-rate cathodes based on $Li_3V_2(PO_4)_3$ nanobelts prepared *via* surfactant-assisted fabrication, *J. Power Sources*, 2011, **196**(7), 3646–3649.

7 T. Jiang, W. Pan, J. Wang, *et al.*, Carbon coated $Li_3V_2(PO_4)_3$ cathode material prepared by a PVA assisted sol–gel method, *Electrochim. Acta*, 2010, **55**(12), 3864–3869.

8 M. Minakshi, P. Singh, N. Sharma, *et al.*, Lithium Extraction–Insertion from/into $LiCoPO_4$ in Aqueous Batteries, *Ind. Eng. Chem. Res.*, 2011, **50**(4), 1899–1905.

9 M. Minakshi, Lithium intercalation into amorphous $FePO_4$ cathode in aqueous solutions, *Electrochim. Acta*, 2010, **55**(28), 9174–9178.

10 F. Sauvage, L. Laffont, J. M. Tarascon, *et al.*, Factors affecting the electrochemical reactivity *vs.* lithium of carbon-free $LiFePO_4$ thin films, *J. Power Sources*, 2008, **175**(1), 495–501.

11 M. Manickam, P. Singh, S. Thurgate, *et al.*, Redox behavior and surface characterization of $LiFePO_4$ in lithium hydroxide electrolyte, *J. Power Sources*, 2006, **158**(1), 646–649.

12 G. J. Wang, N. H. Zhao, L. C. Yang, *et al.*, Characteristics of an aqueous rechargeable lithium battery (ARLB), *Electrochim. Acta*, 2007, **52**(15), 4911–4915.

13 A. Yuan and Q. Zhang, A novel hybrid manganese dioxide/activated carbon supercapacitor using lithium hydroxide electrolyte, *Electrochem. Commun.*, 2006, **8**(7), 1173–1178.

14 A. Eftekhari, Electrochemical behavior of thin-film $LiMn_2$ aqueous media, *Electrochim. Acta*, 2001, **47**, 495–499.

15 J. Lee and S. Pyun, Investigation of lithium transport through $LiMn_2O_4$ film electrode in aqueous $LiNO_3$ solution, *Electrochim. Acta*, 2004, **49**(5), 753–761.

16 J. Luo and Y. Xia, Aqueous Lithium-ion Battery $LiTi_2(PO_4)_3$/$LiMn_2O_4$ with High Power and Energy Densities as well as Superior Cycling Stability, *Adv. Funct. Mater.*, 2007, **17**(18), 3877–3884.

17 F. Risacher and B. Fritz, Origin of Salts and Brine Evolution of Bolivian and Chilean Salars, *Aquat. Geochem.*, 2009, **15**(1–2), 123–157.

18 A. Yaksic and J. E. Tilton, Using the cumulative availability curve to assess the threat of mineral depletion: The case of lithium, *Resour. Policy*, 2009, **34**(4), 185–194.

19 Y. Cao, L. Xiao, M. L. Sushko, *et al.*, Sodium Ion Insertion in Hollow Carbon Nanowires for Battery Applications, *Nano Lett.*, 2012, **12**(7), 3783–3787.

20 P. Senguttuvan, G. Rousse, V. Seznec, *et al.*, $Na_2Ti_3O_7$: Lowest Voltage Ever Reported Oxide Insertion Electrode for Sodium Ion Batteries, *Chem. Mater.*, 2011, **23**(18), 4109–4111.

21 S. Monica and L. L. Shaw, Advances and challenges of sodium ion batteries as post lithium ion batteries, *RSC Adv.*, 2015, **5**, 53129–53154.

22 R. Berthelot, D. Carlier and C. Delmas, Electrochemical investigation of the P2-Na_xCoO_2 phase diagram, *Nat. Mater.*, 2010, **10**(1), 74–80.

23 Y. Cao, L. Xiao, W. Wang, *et al.*, Reversible Sodium Ion Insertion in Single Crystalline Manganese Oxide Nanowires with Long Cycle Life, *Adv. Mater.*, 2011, **23**(28), 3155–3160.

24 T. H. J. U. Sebastian Wenzel, Room-temperature sodium-ion batteries: Improving the rate capability of carbon anode materials by templating strategies, *Energy Environ. Sci.*, 2011, **4**, 3342–3345.

25 S. Komaba, N. Yabuuchi, T. Nakayama, *et al.*, Study on the Reversible Electrode Reaction of $Na_{1-x}Ni_{0.5}Mn_{0.5}O_2$ for a Rechargeable Sodium-Ion Battery, *Inorg. Chem.*, 2012, **51**(11), 6211–6220.

26 M. Sathiya, K. Hemalatha, K. Ramesha, *et al.*, Synthesis, Structure, and Electrochemical Properties of the Layered Sodium Insertion Cathode Material:$NaNi_{1/3}Mn_{1/3}Co_{1/3}O_2$, *Chem. Mater.*, 2012, **24**(10), 1846–1853.

27 S. Oh, S. Myung, J. Hassoun, *et al.*, Reversible $NaFePO_4$ electrode for sodium secondary batteries, *Electrochem. Commun.*, 2012, **22**, 149–152.

28 J. E. C. N. Prabeer Barpanda and A. J. T. Michel Armand, Structural, Transport, and Electrochemical Investigation of Novel $AMSO_4F$ (A = Na, Li; M = Fe, Co, Ni, Mn) Metal Fluorosulphates Prepared Using Low Temperature Synthesis Routes, *Inorg. Chem.*, 2010, **49**, 7401–7413.

29 H. Zhuo, X. Wang, A. Tang, *et al.*, The preparation of $NaV_{1-x}Cr_xPO_4F$ cathode materials for sodium-ion battery, *J. Power Sources*, 2006, **160**(1), 698–703.

30 Y. Kawabe, N. Yabuuchi, M. Kajiyama, *et al.*, Synthesis and electrode performance of carbon coated Na_2FePO_4F for rechargeable Na batteries, *Electrochem. Commun.*, 2011, **13**(11), 1225–1228.

31 T. Jiang, G. Chen, A. Li, *et al.*, Sol–gel preparation and electrochemical properties of $Na_3V_2(PO_4)_2F_3$/C composite cathode material for lithium ion batteries, *J. Alloys Compd.*, 2009, **478**(1–2), 604–607.

32 A. Rudola, K. Saravanan, C. W. Mason, *et al.*, $Na_2Ti_3O_7$: an intercalation based anode for sodium-ion battery applications, *J. Mater. Chem. A*, 2013, **1**(7), 2653.

33 C. Y. Y. L. Wei Wang, Single crystalline $Na_2Ti_3O_7$ rods as an anode material for sodium-ion batteries, *RSC Adv.*, 2013, **3**, 1041–1044.

34 L. Zhao, J. Zhao, Y. Hu, *et al.*, Disodium Terephthalate ($Na_2C_8H_4O_4$) as High Performance Anode Material for Low-

Cost Room-Temperature Sodium-Ion Battery, *Adv. Energy Mater.*, 2012, **2**(8), 962–965.

35 C. Chen, F. Kun, L. Yao, *et al.*, Use of a tin antimony alloy-filled porous carbon nanofiber composite as an anode in sodium-ion batteries, *RSC Adv.*, 2015, **5**, 30793–30800.

36 M. Xu, C. Cheng, Q. Sun, *et al.*, A 3D porous interconnected $NaVPO_4F$/C network: preparation and performance for Na-ion batteries, *RSC Adv.*, 2015, **5**(50), 40065–40069.

37 V. O. Palomares, P. Serras, I. Villaluenga, *et al.*, Na-ion batteries, recent advances and present challenges to become low cost energy storage systems, *Energy Environ. Sci.*, 2012, **5**, 5884–5901.

38 M. Choi, K. Kang, H. Kim, *et al.*, The effect of titanium in $Li_3V_2(PO_4)_3$/graphene composites as cathode material for high capacity Li-ion batteries, *RSC Adv.*, 2015, **5**(7), 4872–4879.

39 M. Ren, Z. Zhou, Y. Li, *et al.*, Preparation and electrochemical studies of Fe-doped $Li_3V_2(PO_4)_3$ cathode materials for lithium-ion batteries, *J. Power Sources*, 2006, **62**(2), 1357–1362.

40 Y. Chen, Y. Zhao, X. An, *et al.*, Preparation and electrochemical performance studies on Cr-doped $Li_3V_2(PO_4)_3$ as cathode materials for lithium-ion batteries, *Electrochim. Acta*, 2009, **54**(24), 5844–5850.

41 C. Dai, Z. Chen, H. Jin, *et al.*, Synthesis and performance of $Li_3(V_{1-x}Mg_x)_2(PO_4)_3$ cathode materials, *J. Power Sources*, 2010, **195**(17), 5775–5779.

42 Q. Kuang, Y. Zhao, X. An, *et al.*, Synthesis and electrochemical properties of Co-doped $Li_3V_2(PO_4)_3$ cathode materials for lithium-ion batteries, *Electrochim. Acta*, 2010, **55**(5), 1575–1581.

43 S. M. Stankov, I. Abrahams, A. Momchilov, *et al.*, Effect of Ti-doping on the electrochemical performance of lithium vanadium(III) phosphate, *Ionics*, 2015, **21**(6), 1501–1508.

44 A. R. Burke, C. R. Brown, W. C. Bowling, *et al.*, Ignition mechanism of the titanium–boron pyrotechnic mixture, *Surf. Interface Anal.*, 1988, **11**(6–7), 353–358.

45 M. Choi, K. Kang, H. Kim, *et al.*, The effect of titanium in $Li_3V_2(PO_4)_3$/graphene composites as cathode material for high capacity Li-ion batteries, *RSC Adv.*, 2015, **5**(7), 4872–4879.

46 G. Li, D. Jiang, H. Wang, *et al.*, Glucose-assisted synthesis of $Na_3V_2(PO_4)_3$/C composite as an electrode material for high-performance sodium-ion batteries, *J. Power Sources*, 2014, **265**, 325–334.